Cellulose (2021) 28:2995–3015
https://doi.org/10.1007/s10570-021-03723-y

ORIGINAL RESEARCH

Oxidized regenerated celluloses to fabricate high fire safety for epoxy resin with super expansion char layer

tao Shi · Shuidong Zhang · Xingxing Shi

Received: 22 October 2020 / Accepted: 23 January 2021 / Published online: 13 February 2021

Abstract Recently, oxidized regenerated celluloses has exhibited superior performance as a carbonization agent for polymers. However, it is a major challenge to fabricate fire safety and intumescent flame-retardant polymer composites with high-efficiency, and "heterogeneous char-forming agent (HCA)" is worth pursuing. Herein, regenerated cellulose (RC) was oxidized by H_2O_2 to achieve oxidized RC (ORC) with high carboxyl content. Interestingly, ORC, the potential HCA, achieved higher catalytic charring effect and lower content of the toxic gas release compared with the presented carbonization agent. 5 wt% ORC and 3.75 wt% microencapsulated ammonium polyphosphate (MFAPP) as intumescent flame retardants (IFR) were utilized to fabricate IFR epoxy resin (EP) (noted as EP/MFAPP/ORC). Amazingly, a super expansion ratio (41.5-fold) intumescent char layer was formed in EP/MFAPP/ORC27 (ORC with 27% carboxyl content) after the cone calorimetry test. Moreover, the peak heat release rate, total heat release and total smoke production of EP/MFAPP/ORC27 largely decreased by 55.6%, 61.8% and 62.2%, respectively. Furthermore, the residual char yield (41.8%) significantly enhanced by 9.7-fold, compared with those of EP. Meanwhile, it achieved 30.3% limiting oxygen index and V-0 burning test, and the flame retardant index (FRI) showed "good" flame-retardant performances. The concept of HCA and flame-retardant mechanism were elaborated by analyzing the evolution process of IFR-EP. These results demonstrate that ORC27, acts as HCA, is a novel and efficient strategy for fabricating fire safety EP with excellent flame-retardant efficiency.

Supplementary Information The online version contains supplementary material available at (https://doi.org/10.1007/s10570-021-03723-y).

t. Shi · X. Shi
College of Mechanical and Automotive, South China University of Technology, Guangzhou 510640, China

S. Zhang (✉)
State Key Laboratory of Bio-Fibers and Eco-Textiles, Qingdao University, Qingdao 250101, China
e-mail: starch@scut.edu.cn

Graphic abstract

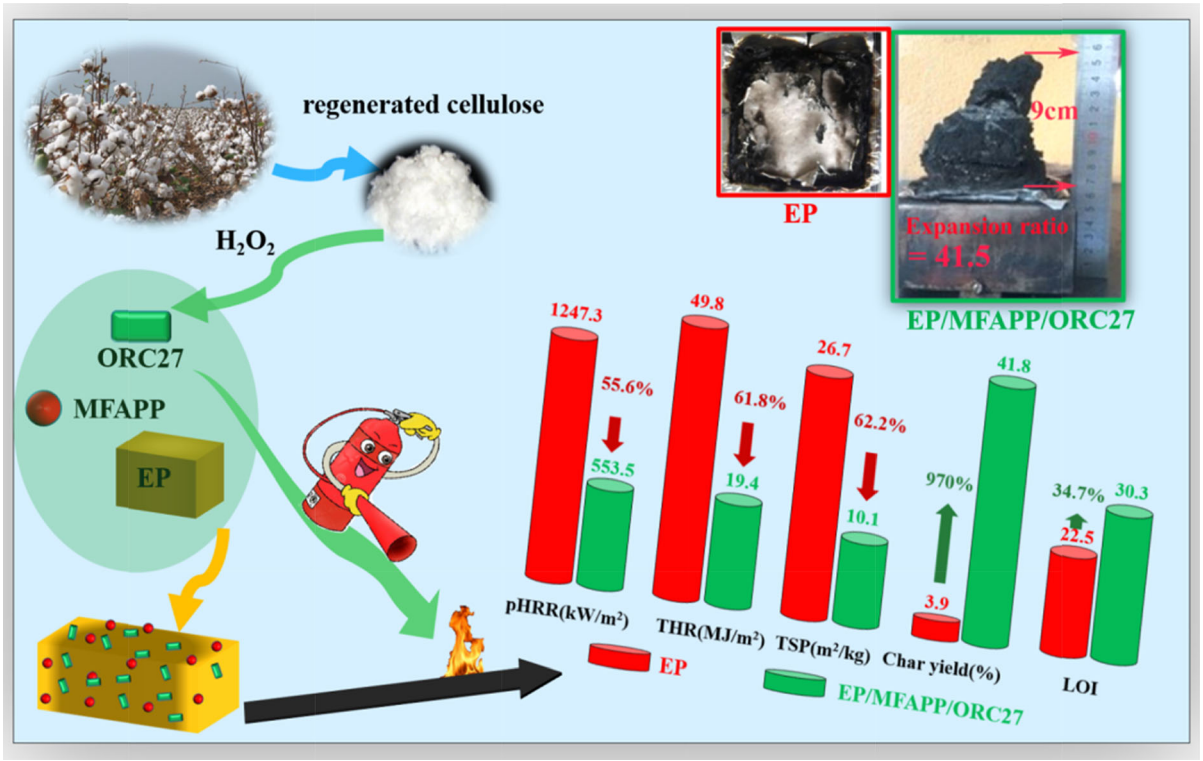

Keywords Oxidized regenerated cellulose · Intumescent flame retardation · Epoxy resin · Heterogeneous char-forming agent · Super expansion ratios

Introduction

Compared to metal and ceramics, polymers possess many merits in light weight, ductility, low cost, and chemical resistance, which make them suitable for wide use in various fields, such as buildings, electric devices, medicines, energy transfer and storage materials (Feng et al. 2018; Qi et al. 2017; Zhang et al. 2015a). Unfortunately, most carbon-based polymers have a high risk of fire which restricts their practical applications. Therefore, the development of a cost-effective and facile method to enhance the fire safety and flame retardancy of the polymers has drawn widespread effort (Wang et al. 2017a). In order to minimize the fire risk and meet the fire safety requirements, many strategies (physical or chemistry) have been developed to prevent the ignition of the polymers and reduce the heat release and toxic smoke release during their combustion (Costes et al. 2017). Among them, the flame-retardant additives exhibit a combination of unique properties, such as increased heat distortion temperature, reduced permeability, improved mechanical properties and endow polymers with multifunctional properties (Bourbigot and Duquesne 2007; Bourbigot et al. 2004). Currently, the traditional flame retardants are metal hydroxides (Song et al. 2008), phosphorus/nitrogen/silicon-containing compounds (Laoutid et al. 2009) and nano dispersed particles [e.g., montmorillonite, clay (Liu et al. 2015) and carbon nanotubes (Ji et al. 2018)].

The intumescent flame retardants (IFR) have drawn much attention due to their unmatched low-smoke, low-toxicity, and high-efficiency properties (Tan et al. 2015; Wang et al. 2011, 2012). Generally, IFR systems usually consist of three fundamental

components, an acid source (e.g., ammonium polyphosphate (APP)), a char forming or carbonization agent (CA) (e.g., pentaerythritol (PER)), and a blowing agent (e.g., melamine (MEL)) (Liu et al. 2011). To date, multiple efforts have been devoted to improve the flame retardant efficiency of IFR, such as new molecules as acid sources (Alongi et al. 2015), new synergistic components (Su et al. 2012), non-polysaccharidic materials (Manfredi et al.2018) and nano-sized components (Alongi et al. 2019; Shen et al. 2013; Xing et al. 2014). Correspondingly, a commonly accepted mechanism of IFR had been proposed. The process of IFR forms char layer by the carbonization from decomposing of carbonization agent, firstly. Then, the foamed cellular charred layer is obtained as the temperature increases, which induces the degradation of the blowing agent and protects the underlying polymer matrix from the heat flux and the flame (Shao et al. 2014a). To achieve highly-efficient and intumescent flame-resistant polymers, charring agent is the key factor to form a compact and homogeneous expanded char layer during the combustion (Tan et al. 2015; Xu et al. 2013). At present, carbonization agents are mainly hydroxyl-containing compounds, such as starch and polyols (Zhao et al. 2016). When the additives (i.e., APP and carbonization agent) are incorporated to the polymer matrix, a stable char layer with a low thermal conductivity can be generated. Then this intumescent charred layer can reduce the heat transfer from the heat source to the polymers and induce the thermal degradation rate and ''fuel flow'' of the polymers to decrease (Bourbigot and Duquesne 2007; Camino et al. 1984, 1985; Vandersall 1971). However, for most IFR, the char layer formed during combustion is easy to break due to the low char strength and complex burning condition, thus limiting the generation of a compact and high intumescent structure (just presented at Fig. 1) (Jung and Bhattacharyya 2018; Li et al. 2019; Pappalardo et al. 2016; Tan et al. 2016a; Wang et al. 2017b). The flame retardancy performances will be decreased and the formed fragile char layer cannot prevent the heat and mass transfer between the gas and condensed phases. Additionally, the mechanism of the expansion process in IFR has not been well addressed. It remains a challenge to fabricate a high-efficiency carbonization agent and develop cost-effective, high-performance, and IFR systems.

Epoxy resin (EP) is one of the typical thermoset polymers in the manufacturing industry, such as casting materials, adhesives, coating, and electronic circuit boards due to its excellent mechanical performance, good adhesive properties, stable chemical resistance, and superb electrical properties (Gu et al. 2016; Jin et al. 2015). Nevertheless, the drawbacks during the combustion of EP (e.g., high flammability, large smoke generation, and toxic gases) severely restrict its further potential applications in composites (Zhang et al. 2015b; Zhou et al. 2019). Therefore, many efforts have been made to improve the flame retardant performance of EP, such as the functionalized nano-particles, (Kalali et al. 2015; Yang et al. 2020) the selection of blowing agent (Zhang et al. 2016, 2018) and curing agent (Ke et al. 2010; Li et al. 2019) etc. But the in-depth investigations of IFR have never been reported, to our knowledge.

In our previous research, we had developed a facile and green approach to fabricate oxidized starch (Zhang et al. 2009, 2015b) and oxidized regenerated cellulose (ORC) with controlled carboxyl content (ranged from 13 to 35%) via H_2O_2 (Wen et al. 2019). Meanwhile, the oxidized wood flour were acted as the new functional filler for poly(lactic acid) composites to further improve their flame retardancy (Yang et al. 2019; Zhang et al. 2019). Simultaneously, our low-cost green oxidation system can selectively oxidize the cellulose in the C-6 hydroxyl group with high carboxyl content, and the most noticeable point to highlight is that ORC exhibits high residual char and low combustible gas release during the thermal decomposition. Meanwhile, oxidized starch and ORC with 15.6% carboxyl content are proved to be a highly-efficient carbonization agent for EP (Peng et al. 2017; Zhang et al. 2015b). Interestingly, ORC tends to exhibit a higher catalytic charring effect, while lower content of the toxic gas release compared with the traditional CA. Notably, ORC can be considered as an impurity in the EP matrix and the carboxyl group in ORC may promote the cleavage of the ester bond in the EP molecular chain. Therefore, inspired by the heterogeneous nucleation during crystallization, ORC is hoped to act as a heterogeneous catalysis in the formation of the char layer. Accordingly, we first proposed the concept of "heterogeneous char-forming agent (HCA)". Consequently, in this work, we develop the green ORC with high carboxyl content (5 wt%) and microencapsulated

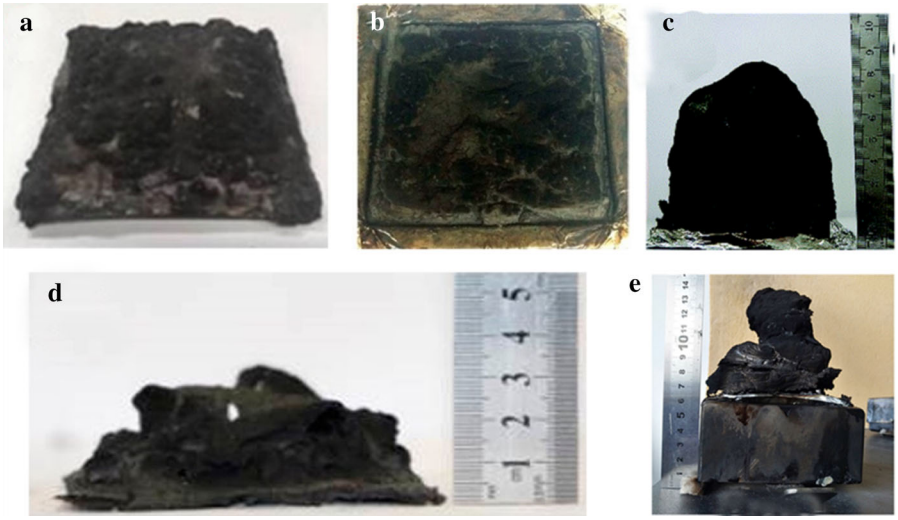

Fig. 1 Digital photos after CCT test of different IFR systems **a** ET/OSEP (Pappalardo et al. 2016), **b** APP/PER/Uracil (Jung and Bhattacharyya 2018), **c** PAz-APP (Tan et al. 2016a), **d** FR wool L-PA (Wang et al. 2017b), and **e** APP/CaG (Li et al. 2019)

ammonium polyphosphate (MFAPP) (lower than 3.75 wt%) to fabricate IFR-EP, fantastic, a stable, compact, and intumescent char layer with a super expansion ratio can be achieved during the cone calorimeter test (CCT), successfully. Moreover, the IFR-EP also achieve high flame retardancy (V-0 with LOI of 30.3%) with the significant decrease in total heat release (THR) and total smoke production (TSP), simultaneously. The mechanism of ORC influences on the formation process of IFR char layer is also investigated and proposed to perfect the IFR theory. Additionally, the intumescent char structure under different carbonization temperatures (e.g., 280, 340, 420, and 550 °C) and flame-retardant mechanism of EP/MFAPP/ORC are investigated.

Experimental section

Materials

Regenerated cellulose (RC) yarn was provided by Ningbo Xuyi Textile Co., Ltd. Epoxy resin (EP, CYD-128) was purchased from China Petrochemical Corporation (Yueyang, China). Polyether amine curing agent (D230, Baxxodur®EC301) was purchased from BASF SE; Ammonium polyphosphate (APP) was supplied by Sichuan Haiwang flame retardant materials Co. (Dujiangyan, China). All other chemicals and solvents were of analytical grades (99.5%) and used as received.

Fabrication of ORC with different carboxyl content

50.0 g Oxidized regenerated cotton cellulose (ORC) was prepared by the oxidation of pretreated recyclable cellulose (PRC), with hydrogen peroxide as the oxidant and $CuSO_4$ as the catalyzer (Wen et al. 2019). Different proportions of hydrogen peroxide (the molar ratios of H_2O_2 and RC ranged from 1.0 to 3.0) was added to 150 ml deionized water, then the pH was adjusted to 6.1 with sodium hydroxide. Next, PRC and 50 mg $CuSO_4$ (0.1% wt. based on ORC) were added to the mixture. The mixture was kept at 35 ± 0.1 °C for 48 h. When the reaction was completed, the oxidized fibers were filtered off, and then washed with deionized water and dried in the vacuum oven at 40 °C and 80 °C for 24 h, respectively. Finally, the product was obtained after pulverization and ORC with 13%, 27% and 35% carboxyl content were named as ORC13, ORC27 and ORC35, respectively.

Preparation of MFAPP

MFAPP was prepared in our lab according to the method of Yang et al. (Yang et al. 2014). Briefly, 63 g melamine, 110 ml formaldehyde solution (37%), and 250 ml distilled water were placed into a triple-necked flask, which was equipped with a condenser and a stirrer. The mixture was adjusted to pH 8–9 by adding 25% ammonia in water, and then the temperature was heated to 85 °C and maintained for about 15 min.

Next, the solution was transferred to another triple-necked flask containing 100 g APP-II and 100 ml distilled water. The temperature in this system was maintained at 85 °C for 2.5 h. Then the mixture was filtered, washed with distilled water, and dried at 100 °C. Finally, the MFAPP-II powder was obtained. The phosphorus (P_2O_5) contents of MFAPP-II and APP-II were determined using a weighing method. The phosphorus content in APP-II and MFAPP-II was 70.36% and 29.63%, respectively. Therefore, the APP-II content in MFAPP-II was about 42.11%.

Preparation of IFR-EP

To evaluate the flame-retardant efficiency of ORC in polymers, MFAPP and ORC with different carboxyl contents are incorporated into the EP matrix to fabricate IFR-EP. A typical case (epoxy-based composites (EP/MFAPP/ORC) containing 5 wt% ORC and 3.75 wt% MFAPP) was prepared according to the following procedures. 22.72 g curing agents (D230) and 68.53 g epoxy resin (EP) were added into a plastic beaker and mixed for 10 min. The mixture was placed in a vacuum chamber at 40 °C for 40 min. Then, 5.0 g ORC and 3.75 g MFAPP were mixed with the pre-mixture for 3 min. Subsequently, the mixture was mixed under mechanical stirring with a speed of 2000 rpm for 7 min until a homogeneous mixture was formed. Then, the mixture was poured into molds. Finally, the EP/MFAPP/ORC was cured at 60 °C for 2 h and at 85 °C for 1.5 h, respectively. After curing, the composites were permitted to cool to room temperature. PER, a traditional char forming agent in the IFR system, is utilized to prepare EP/MFAPP/PER as the control sample. The EP/MFAPP/PER and EP/MFAPP/RC were prepared by the analogous procedure. ORC with 13%, 27% and 35% carboxyl content as carbonization agent in EP/MFAPP/ORC was named as EP/MFAPP/ORC13, EP/MFAPP/ORC27 and EP/MFAPP/ORC35, respectively.

Kinetic analysis

The Friedman method is the most direct way to get the activation energy based on equal conversion thermal analysis. The equal conversion integral method is also called the Flynn–Wall–Ozawa method (FWO method) (Ozawa 1965; Flynn and Wall 1966).

The Flynn–Wall–Ozawa method was used to further elucidate the thermal degradation behaviors of EP/MFAPP/PER and EP/MFAPP/ORC27.

$$logF(\alpha) = log\frac{AE}{R} - log\beta - 2.315 - 0.4567\frac{E}{RT} \quad (1)$$

where A was the pre-exponential factor, E was the activation energy, R was the gas constant, β was the heating rate, T was the absolute temperature and $F(\alpha)$ was the function of degree of conversion (weight loss).

This method could be used to determine the activation energy from TGA results, which was only relevant to the temperatures at a constant degree of conversion from several integral thermograms at different heating rates. The activation energy for different conversion values was calculated from the $\log\beta$ versus $1/T$ plot. The TGA curves of EP/MFAPP/PER and EP/MFAPP/ORC27 at different heating rates under nitrogen were illustrated in Fig. S1. Activation energies at 5, 10, 20, 30, 40, 50 and 60% conversion were calculated, respectively. Fig. S2 showed the best-fit lines of the $\log\beta$ versus $1/T$ plots which were nearly parallel, with correlation coefficients above 0.99.

Measurements

Limit oxygen index (LOI) tests were conducted on a JF-3 oxygen index instrument (Jiangning Analysis Instrument Factory, China), according to GB/T2406-93 standard. The dimensions of all samples were 120 × 6.5 × 3.0 mm^3. Vertical burning ratings (UL-94) of all samples were measured on a CZF-2 instrument (Jiangning Analysis Instrument Factory, China) with sample dimensions of 130 × 12.5 × 3 mm^3. The burning time was recorded from the UL-94 tests based on average burning time of five specimens. CCT is an effective method to assess the flammability behavior of materials. Heat release rate (HRR), peak heat release rate (pHRR), total heat release (THR), and total smoke production (TSP) achieved from CCT are the key parameters for fire hazard evaluation of materials. The combustion properties of EP composites were carried out on a cone calorimeter based on ASTM E1354/ISO5660. Every specimen with the sizes of 100 × 100 × 1.5 mm^3 (the origin volume noted as V_0 and the value was 15 cm^3) wrapped in an aluminum foil was exposed horizontally to a heat flux of 35 kW/m^2. Notably, the standard samples with

3.0 mm thickness are not suitable for this test due to the high expansion ratios of the samples. To calculate the expansion ratio of IFR-EP, we simulated a round table model to calculate the volume V_1, just presented at Scheme 1. After the cone calorimeter test, a ruler was used to measure the bottom radius (R), top radius (r) and height (H) of the expanded carbon. V_1 and expansion ratio (Er) were calculated according to the following equations:

$$V_1 = 1/3\pi h(R\text{^}2 + r\text{^}2 + R \cdot r) \quad (2)$$

$$Er = \frac{V_1}{V_0} - 1 \quad (3)$$

Fourier transform infrared (FTIR) spectra were recorded by a Nicolet FTIR 170SX spectrometer (Nicolet, America) using the KBr disk, and the wave number range was set from 4000 to 500 cm^{-1}. Thermogravimetric analysis-infrared spectrometry (TGA-IR) was performed using the TGA Q5000 IR thermogravimetric analyzer that was linked to the Nicolet 6700 FTIR spectrophotometer. About 5.0 mg of the sample was placed in an alumina crucible and heated from 40 to 800 °C. The heating rate was 10 °C/min (nitrogen atmosphere, flow rate of 50 mL/min). Thermogravimetric analysis/mass spectrometry (TGA-MS) measurements were carried out using a 409 PC thermal analyzer (Netzsch, Germany) coupled with a QMS403C instrument (Netzsch, Germany). About 10 mg of each sample was heated from 40 to 800 °C at a heating rate of 10 °C/min under N_2 atmosphere. Mass scanning was carried out over the range m/v 2–100. The morphology of the samples was obtained by a Quanta 200 scanning electron microscope (SEM) with accelerated voltage of 15 kV and 18 kV. The samples were sputtered with gold using the ion sputter coater. X-ray photoelectron spectroscopy (XPS) spectra of the samples were recorded by a VG Escalab mark II spectrometer (VG Scientific Ltd., UK), using Al KR excitation radiation (1253.6 eV), respectively. The assigned spectra peaks were ascertained through the NIST X-ray Photoelectron Spectroscopy Database (https://srdata.nist.gov/xps/selEnergyType.aspx).

Results and discussions

Flame retardancy

The LOI and UL-94 tests are utilized to evaluate the flame-retardant performances of EP and IFR-EP samples, and the related data are listed in Table 1. The results demonstrate that EP/MFAPP/ORC can achieve high flame retardancy, while EP and EP/MFAPP/RC are highly flammable, indicating that the introduction of RC cannot effectively improve the flame retardancy of EP. With the increase of MFAPP content, both the UL-94 rating and LOI value of IFR-EP rise. For example, the LOI of EP/MFAPP/ORC27 (91.25/2.5/6.25 wt%) is 27.5%, while the LOI of EP/MFAPP/ORC27 (88.75/5/6.25 wt%) increases to 31.2% with UL 94 V-0 when the content of MFAPP is 5 wt%. As the MFAPP content increases, EP/MFAPP/ORC27 (88.75/6.25/6.25 wt%) obtains V-0 level with 32.9% LOI. It can be seen that with the increase of MFAPP content, the flame-retardant performances of IFR-EP are improved, significantly.

According to Table 1, IFR-EP samples exhibit excellent flame retardancy with the minimum amount (3.75%/5%, MFAPP/ORC) of intumescent flame retardancy additives. In this combination, EP/

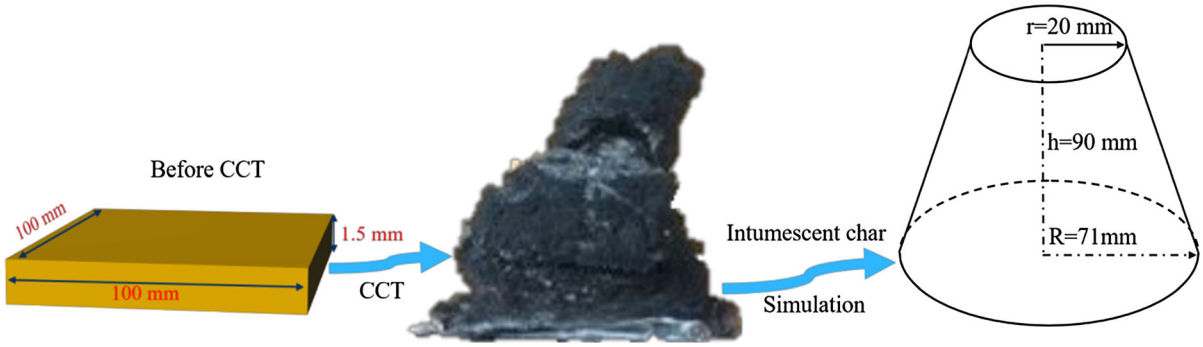

Scheme 1. The calculation of the expansion ratio (Er) of IFR-EP

Table 1 LOI and vertical test of IFR-EP and pure epoxy resin

Samples	LOI	UL-94
EP	22.5	No rating
EP/MFAPP/PER (87.5/6.25/6.25 wt%)	31.7	V-0
EP/MFAPP/RC (87.5/6.25/6.25 wt%)	24.9	No rating
EP/MFAPP/ ORC13 (87.5/6.25/6.25 wt%)	25.8	V-0
EP/MFAPP/ ORC27 (87.5/6.25/6.25 wt%)	32.9	V-0
EP/MFAPP/ ORC35 (87.5/6.25/6.25 wt%)	33.3	V-0
EP/MFAPP/PER (88.75/5/6.25 wt%)	28.8	V-1
EP/MFAPP/RC (88.75/5/6.25 wt%)	24.1	No rating
EP/MFAPP/ORC13 (88.75/5/6.25 wt%)	25.8	V-0
EP/MFAPP/ORC27 (88.75/5/6.25 wt%)	31.2	V-0
EP/MFAPP/ORC35 (88.75/5/6.25 wt%)	30.7	V-0
EP/MFAPP/PER (91.25/3.75/5 wt%)	29.0	V-1
EP/MFAPP/RC (91.25/3.75/5 wt%)	23.6	No rating
EP/MFAPP/ORC13(91.25/3.75/5 wt%)	29.0	V-1
EP/MFAPP/ORC27 (91.25/3.75/5 wt%)	30.3	V-0
EP/MFAPP/ORC35 (91.25/3.75/5 wt%)	29.3	V-0
EP/MFAPP/PER (91.25/2.5/6.25 wt%)	21.5	No rating
EP/MFAPP/RC (91.25/2.5/6.25 wt%)	21.2	No rating
EP/MFAPP/ORC13 (91.25/2.5/6.25 wt%)	21.4	No rating
EP/MFAPP/ORC27 (91.25/2.5/6.25 wt%)	27.5	No rating
EP/MFAPP/ORC35 (91.25/2.5/6.25 wt%)	24.5	No rating

MFAPP/PER does not achieve the UL-94 V-0 rating in the vertical combustion test when it used as the control. Whereas in fact, with the increased carboxyl contents of ORC, the LOI values of EP/MFAPP/ORC increase. The LOI values of EP/MFAPP/ORC27 and EP/MFAPP/ORC35 are 30.3% and 29.3%, which are higher than that of EP/MFAPP/PER and EP/MFAPP/RC. It has previously been observed that a polysaccharide with carboxyl groups, tends to endow a higher catalytic charring effect than a traditional char forming agent for IFR-EP (Peng et al. 2017; Zhang et al. 2015b). Further analysis shows that ORC is significantly more effective to improve the LOI value of EP than PER.

In order to analyze the combustion behaviors in CCT, the HRR, pHHR, and TSP curves of neat EP and IFR-EP are shown in Fig. 2, and the corresponding data are listed in Table 2. It can be observed that EP burns rapidly, and its PHRR and THR are 1247.3 kW/m^2 and 49.8 MJ/m^2, respectively. The PHRR value of EP/MFAPP/PER slightly decreases to 1022.2 kW/m^2 after the introduction of MFAPP/PER, while significantly decreases to 553.5 kW/m^2 as the introduction of ORC27. It is interesting that EP/MFAPP/ORC27 achieves the lowest THR (19.4 MJ/m^2) and TSP (10.1 m^2/kg) of all samples. Moreover, the char yield of EP/MFAPP/ORC is much higher than that of EP/MFAPP/PER and EP/MFAPP/RC, proved the enhanced char formation of IFR-EP samples due to the introduction of ORC.

The Flame Retardancy Index (FRI) was used to further elucidate the flame retardancy performance of EP-IFR. Among them, flame retardancy are defined as "poor" (FRI < 0), "good" ($0 <$ FRI < 10) and "excellent" ($10 <$ FRI < 100) (Vahabi et al. 2019), respectively. According to the method, the EP/MFAPP/ ORC27 exhibits the best flame retardancy with the largest FRI value, as shown in Fig. 2D.

Digital photographs of the char residues for all samples after CCT are presented in Fig. 3. It is observed that both EP/MFAPP/PER and EP/MFAPP/RC gain small amount of char residue after combustion. It is interesting that an intumescent char layer with a thick and compact char layer is formed after the combustion of the EP/MFAPP/ORC, with a marked increase in the expansion ratio. The super expansion char layer of EP/MFAPP/ORC27 (about 41.5-fold) can protect EP to prevent the transmission of heat and oxygen, inhibit the volatilization of the combustible gases feeding back to the burning zone, thus reduce the flammability of EP (Nie et al. 2009; Tan et al. 2015, 2016a, 2016b). The variations in the morphology of char residue are in accordance with the results of PHRR, THR and TSP.

Consequently, based on the results of flame retardancy for IFR-EP, it can be concluded that (1) ORC is much more effective than PER or RC in improving the fire resistance of IFR-EP; (2) EP/MFAPP/ORC can not only improve the quantity but also the quality of the char residue during combustion.

Thermal properties

The thermal stability of RC and ORC with different carboxyl contents were evaluated by TGA in nitrogen atmosphere and presented in Fig. S3, the precise $T_{5\%}$ and T_{max} of all samples are listed in Table S1. Interestingly, compared with that of RC, the char residue of ORC35 at 600 °C increases from 15.5 to 27.2 wt%, significantly. The reason can be attributed

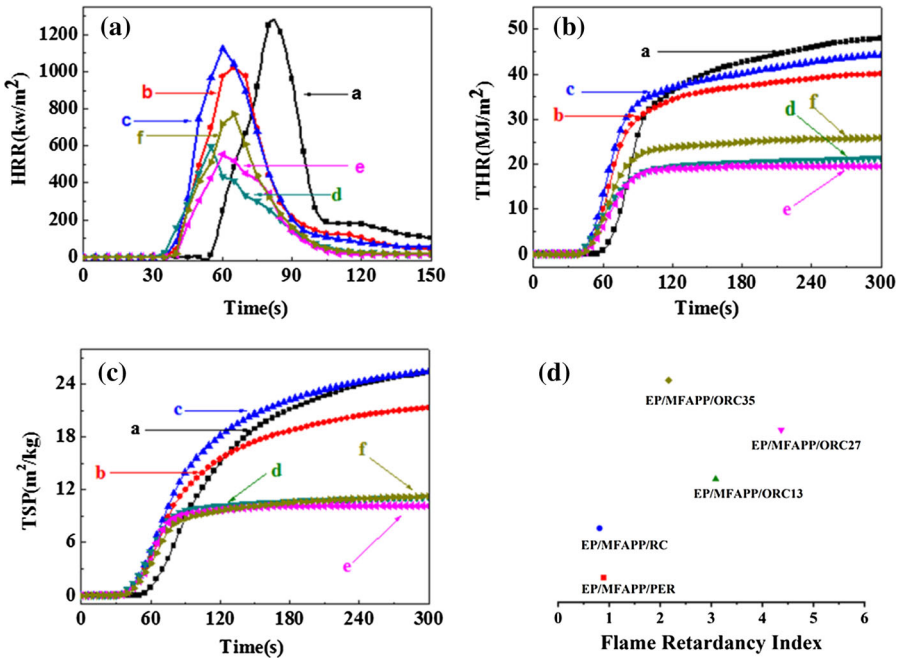

Fig. 2 The curves of EP and IFR-EPs obtained from cone calorimeter test: **A** HRR, **B** THR, **C** TSP, (a) EP, (b) EP/MFAPP/PER, (c) EP/MFAPP/RC, (d) EP/MFAPP/ORC13, (e) EP/MFAPP/ORC27 and (f) EP/MFAPP/ORC35. **D** The calculated FRI for EP

Table 2 Cone calorimeter parameters of IFR-EP and pure epoxy resin

Samples	TTI (s)	pHRR (kW/m^2)	THR (MJ/m^2)	TSP (m^2/kg)	Char yield (%)	Expansion ratio
EP(a)	49	1247.3	49.8	26.7	3.9	–
EP/MFAPP/PER(b)	**29**	**1022.2**	**40.4**	**21.9**	**13.2**	**–**
EP/MFAPP/RC(c)	31	1122.9	43.1	26.1	11	–
EP/MFAPP/ORC13(d)	31	597.9	21.3	11.1	35.2	22.4
EP/MFAPP/ORC27(e)	**37**	**553.5**	**19.4**	**10.1**	**41.8**	**41.5**
EP/MFAPP/ORC35(f)	34	772.0	25.8	11.2	27.9	17.6

(1) Time to ignition (TTI, s): under the same irradiation power and sample thickness, the longer TTI means it is harder to ignite the material. For flame-retarding polymers, they often decompose in advance due to the addition of flame retardant, thereby shortening the TTI. Therefore, the shorter TTI does not mean that the flame retardancy of materials becomes worse

(2) Heat release rate (HRR, KW/m^2): it is defined as the heat release per unit time and unit surface area during the cone calorimetry test. Particularly, the peak value of HRR (PHRR) or its maximum (HRRmax) is used to evaluate the fire performance of materials

(3) Total heat release (THR, kJ/m^2): the total calorific value released per unit area after the combustion process for materials, which can be calculated according to the integration of the HRR vs. time

to the presence of terminal carboxyl groups which will play a key role in catalyzing the dehydration of glucose units. Furthermore, we also investigate the thermal degradation behaviors of MFAPP/PER, MFAPP/RC, MFAPP/ORC13, MFAPP/ORC27 and MFAPP/ORC35 in both nitrogen and air atmospheres by TGA. The TGA and DTG curves of samples are shown in Fig. S4, and the corresponding data are summarized in Table S2. Compared with that of MFAPP/PER, both MFAPP/ORC27 and MFAPP/ORC35 display higher thermal stability and char residue, correspondingly. Consequently, ORC can serve as a high efficiency char-forming agent for IFR-EP.

Furthermore, the thermal stability of EP/MFAPP/ORC was evaluated to reveal the reasons for the high flame retardancy in EP/MFAPP/ORC. Figure 4a, b shows the TGA curves of specimens evaluated under nitrogen, and the detailed data, including $T_{5\%}$ and T_{max} are listed in Table S3. Undoubtedly, the

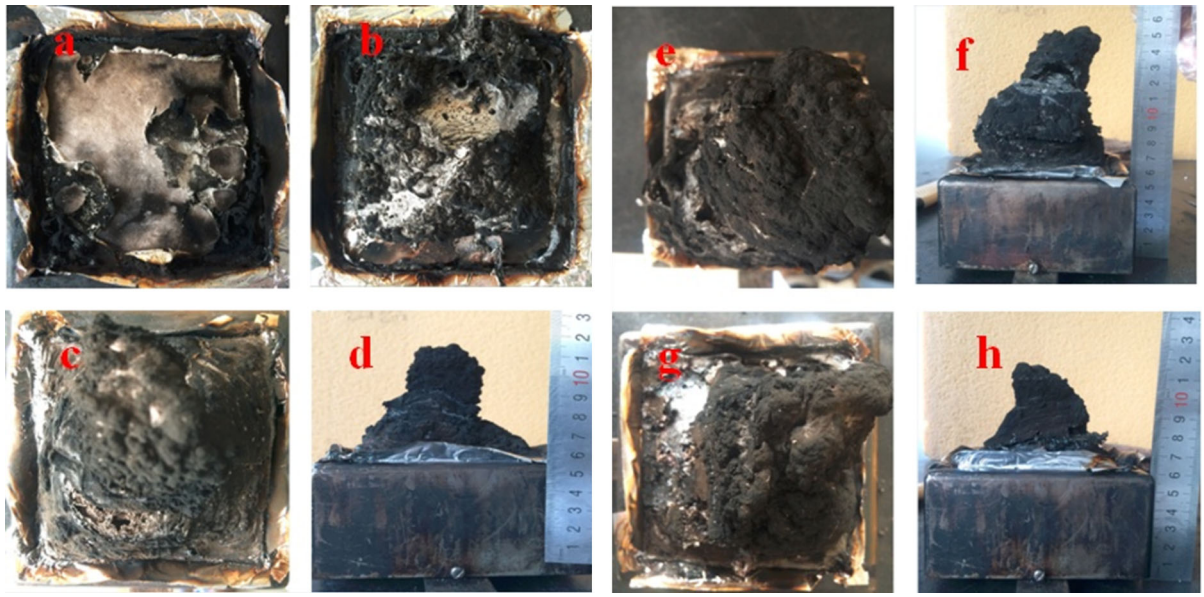

Fig. 3 Digital photographs of burning residues from Cone calorimeter test: **a** EP/MFAPP/PER, **b** EP/MFAPP/RC, **c**, **d** EP/MFAPP/ORC13, **e**, **f** EP/MFAPP/ORC27, **g**, **h** EP/MFAPP/ORC35

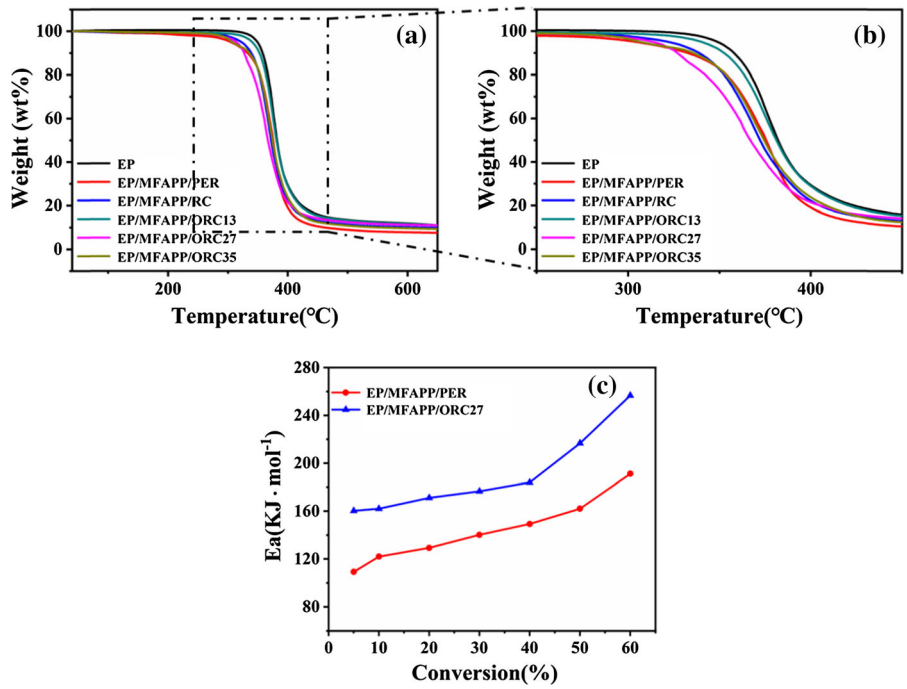

Fig. 4 **a**, **b** TG curves at a heating rate of 10 °C·min^{-1} under N_2 atmospheres. **c** Activation energy of EP/MFAPP/PER and EP/MFAPP/ORC27 as a function of conversion

incorporation of IRFs reduces the thermal stability of EP (Jian et al. 2019).

The activation energy reflects the difficulty of the material decomposition and char formation. Herein, to elucidate the variations in activation energy (E) of EP/MFAPP/PER and EP/MFAPP/ORC27 influence on the structure of intumescent char layer, the E data as a function of conversion are displayed in Fig. 4c and Table S4. It can be seen that the apparent activation energy of EP/MFAPP/ORC27 is much higher than that

of EP/MFAPP/PER. Hence, there are much higher energy barriers to overcome for EP/MFAPP/ORC27 than that of EP/MFAPP/PER, meaning the decomposition of EP/MFAPP/ORC27 becomes more difficult, and a more stable residue is generated. As determined from the corresponding TGA curves, EP/MFAPP/ORC27 exhibits an increased initial decomposition temperature, a decreased maximum decomposition rate, while an enhanced char residue. The phenomenon maybe an important factor to promote EP/MFAPP/ORC27 to achieve high expansion char layers. To reveal the mechanism of char formation of the ORCs in EP, the dynamic analysis for both gas phase and char layer structure of EP/MFAPP/ORC had been adopted.

Gas phase analysis

Generally, the blowing gases (originated from gas sources), such as the release amount and rate, act as a key function to form a porous char layer on the surface of materials for IFR (Wang et al. 2019; Xu et al. 2019). Herein, to explore the flame retardant and thermal degradation mechanisms of EP/MFAPP/ORC, TGA-IR and TGA-MS were used to identify the volatilized products generated from neat EP and IFR-EP during the thermal degradation. The 3D TGA-IR spectra of the gas phase of the thermal degradation are adopted in the study. Peaks located (Fig. 5) in the regions of 3600–4000 cm^{-1}, 2750–3150 cm^{-1}, 2250–2400 cm^{-1}, 1400–1650 cm^{-1}, 1100–1300 cm^{-1}, and 600–800 cm^{-1} are attributed to water, carbon dioxide and compounds containing the aromatic ring, respectively. The addition of IFR does not vary the decomposition products, while changes the gas release amounts. Compared with that of EP/MFAPP/PER, the gas release amounts of EP/MFAPP/ORC decrease. Moreover, for EP/MFAPP/ORC, the gas release amounts decrease as the carboxyl contents of ORC increase. For IFR, the high gas release amounts also evoke the char layers to break, while the low one will cause the lower expansion rate

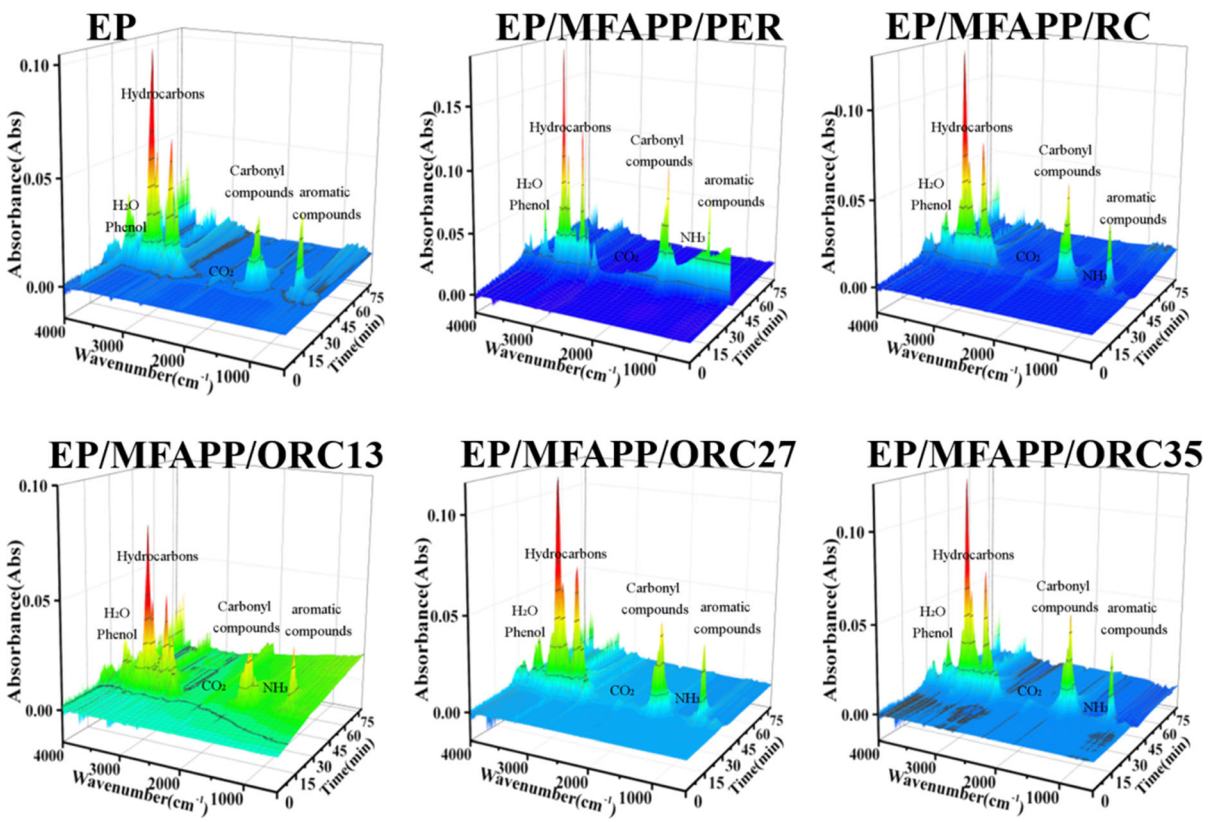

Fig. 5. 3D surface graph for the FTIR spectra of the evolved gases products

of char layers. Based on the flame retardant of EP/MFAPP/ORC, we can deduce that EP/MFAPP/ORC27 owns an optimal gas release amount, which endows it to achieve high flame-retardant performances.

In order to better understand the detailed thermal degradation process of neat EP and IFR-EP, the released gases under different temperatures (250, 280, 340, 420 and 550 °C) are also investigated. As shown in Fig. 6, the corresponding characteristic peaks are shown in Table S5, the peaks at 1602, 1510, and 746 cm^{-1} are corresponding to volatile aromatic compounds. These peaks reflect the chain scission of phenol or bisphenol A and its derivatives or polyester fragments. For EP/MFAPP/PER, a peak near 1750 cm^{-1} is observed as the temperature increases to 250 °C, which may be ascribed to the sublimation of PER from EP matrix. For EP or EP/MFAPP/ORC, no pyrolysis gases can be detected when the temperature is lower than 280 °C, however. When the temperature increases from 280 to 550 °C, both EP/MFAPP/ORC13 and EP/MFAPP/ORC27 exhibit a significant high pyrolysis release rate at 340 °C and decrease at 420 °C, then keep a stability of pyrolysis release at 550 °C. However, EP/MFAPP/PER, EP/MFAPP/RC and EP/MFAPP/ORC35 show a different trend of pyrolysis release rate: all of them display continuous high pyrolysis release rate from 340 to 420 °C, then decrease at 550 °C. As shown in Table 3, the volatile products (e.g., hydrocarbons, CO_2, and aromatic compounds) for EP/MFAPP/ORC27 are in lower content than those of EP/MFAPP/PER. The reason is attributed to the fact that more aromatic compounds in EP/MFAPP/ORC27 are favored to converting to solid carbon than those of EP/MFAPP/PER. This merit will promote more carbon to participate in the formation of the char layer when EP/MFAPP/ORC is ignited.

To analyze how ORC influences the pyrolysis products of EP, TGA-MS is utilized to investigate the degradation and pyrolysis mechanism of EP/MFAPP/ORC. Several intensive signals are detected at m/z = 18, 44, 47, 63, and 94. The H_2O molecule is associated with a signal at m/z = 18, while the m/z = 44 and 94 are attributed to CO_2 and phenol, respectively. Meanwhile, fragments with m/z = 47 and 63 are ascribed to OP^+ and O_2P^+ (Ding et al. 2017). TGA-MS of EP and IFR-EP are presented at

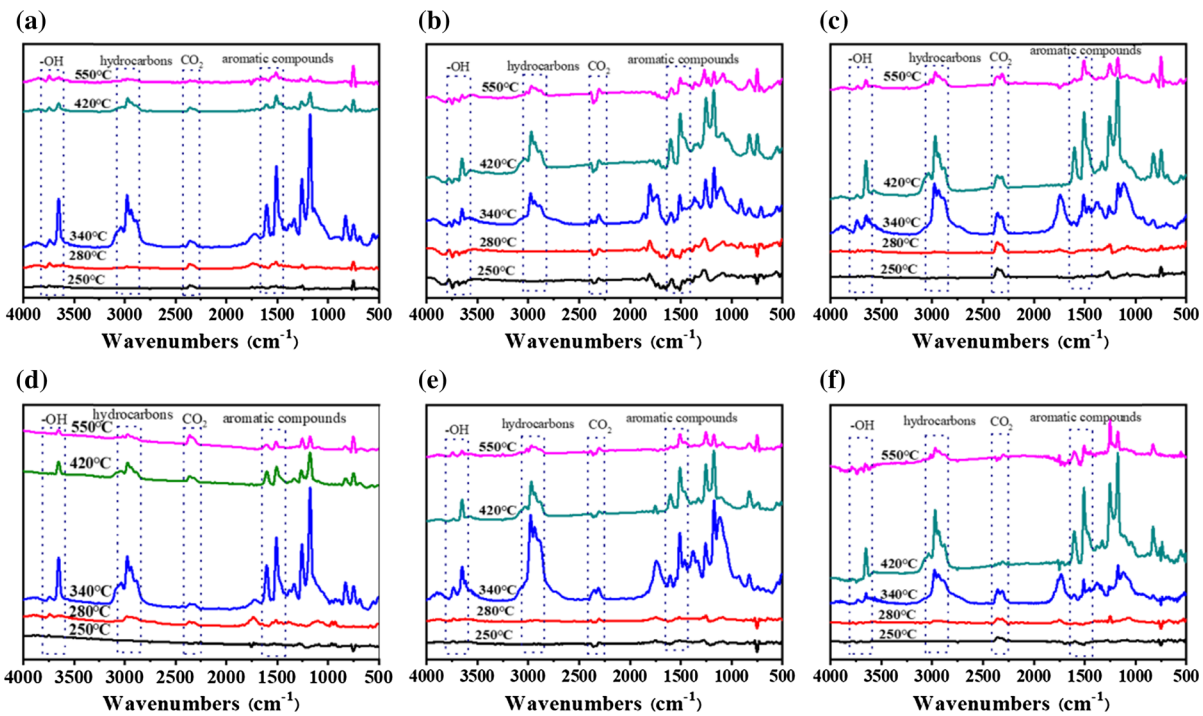

Fig. 6 The FTIR spectra of the gas phase in the thermal degradation of **a** EP, **b** EP/MFAPP/PER, **c** EP/MFAPP/RC, **d** EP/MFAPP/ORC13, **e** EP/MFAPP/ORC27, and **f** EP/MFAPP/ORC35 at different temperatures

Table 3 The content of pyrolysis products for EP compounds at maximum decomposition rate

Samples	Hydrocarbons (%.)	CO_2 (%)	Aromatic compounds (%)
EP	18.89	0.73	4.16
EP/MFAPP/PER	27.48	0.73	2.91
EP/MFAPP/RC	30.65	0.82	2.57
EP/MFAPP/ORC13	21.66	0.70	3.01
EP/MFAPP/ORC27	26.74	0.39	2.08
EP/MFAPP/ORC35	32.05	0.58	2.80

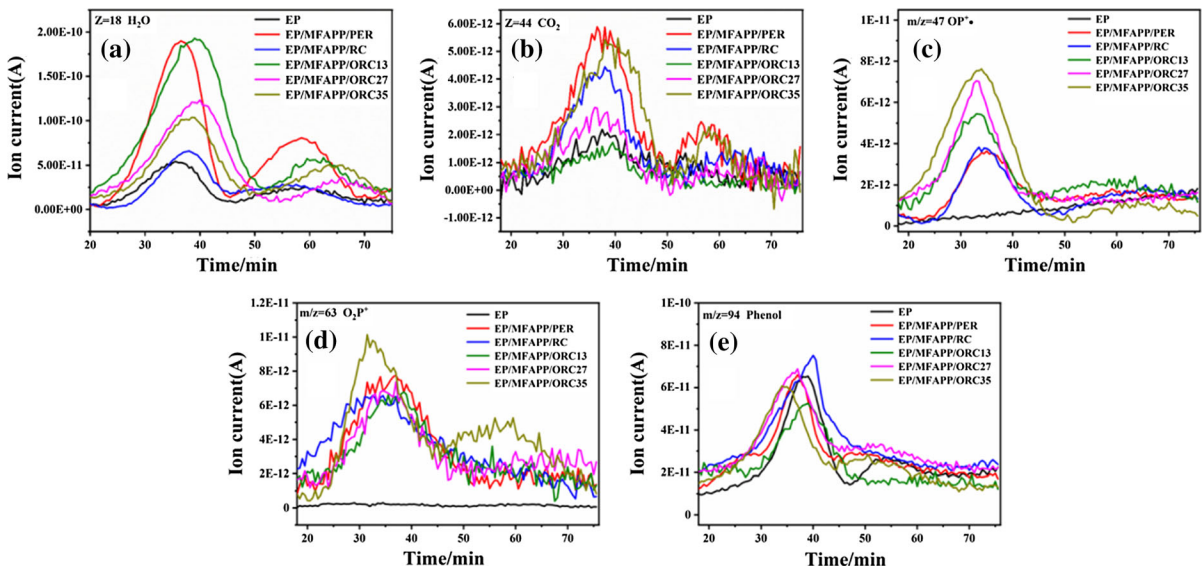

Fig. 7 The ion current of the major gaseous species released from EP and IFR-EP thermal pyrolysis in nitrogen atmosphere

Table 4 TGA-MS integrated intensity of different ion current curves

Samples	H_2O (E-10)	CO_2 (E-10)	OP^+•(E-10)	O_2P^+ (E-10)	Phenol (E-10)
EP	1.25	5.82	0	0	1.58
EP/MFAPP/PER	3.76	12.6	1.06	2.14	1.79
EP/MFAPP/RC	1.38	9.01	1.05	2.26	2.22
EP/MFAPP/ORC13	4.28	4.02	1.35	2.04	1.05
EP/MFAPP/ORC27	2.69	6.51	1.37	2.24	2.13
EP/MFAPP/ORC35	2.52	11.88	1.52	2.50	1.74

Fig. 7 and the data are listed in Table 4. Compared with that of EP, the introduction of IRF can promote the release amounts of H_2O and CO_2, which may act as blowing gases to form the expanded char layers. Meanwhile, the signals of OP^+ and O_2P^+ just presented in the curves of EP/MFAPP/PER and EP/MFAPP/ORC. EP/MFAPP/PER obtains the highest ion current of pyrolysis products, which is good agreement with the TGA-IR measurement. The CO_2 and phenol outputs of EP/MFAPP/ORC27 are clearly less than those of EP/MFAPP/PER, which may assign to the greater number of carbon residue's formation. Furthermore, Fig. 7c, d display some interesting information, for example, they show that the OP contents increase when with the carboxyl contents of ORC range from 13 to 35%, indicating that the presence of carboxylic acid (pyrolysis produce from ORC) can promote the generation of OP ions. The existences of OP^+ and O_2P^+ can accelerate the radical recombination, thereby causing the quenching effect

in the gaseous phase and improve the flame retardancy performances of EP/MFAPP/ORC. Summary, all of the TGA-MS results are in good agreement with the TGA-IR data and reveal that EP/MFAPP/ORC27 shows a high OP^+ and O_2P^+content in the gas phase with high organic carbon compounds converting to solid carbon.

Char layer structure analysis

To reveal how the char-layer structure varies with the increase of temperature, FTIR, XPS, Raman spectroscopy and SEM were investigated. Figure 8a, b shows the FTIR spectra of the char layer for the EP/MFAPP/PER and EP/MFAPP/ORC27 at different temperatures. The char layers of EP/MFAPP/PER and EP/MFAPP/ORC27 display similar curve features when the temperature is 340 °C. Detailly, the peaks at 2200–1800 cm^{-1} and 1618 cm^{-1} are assigned to $C=N^+$–H and C=N, respectively. Moreover, the absorption peak near 1500 and 1450 cm^{-1} indicates the formation of polyaromatic carbon. Additionally, the peaks at around 1262–900 cm^{-1} are ascribed to the vibration of P–O–C, C–N, P–O–P and P-O, respectively, and the peaks of P–N–C are observed at 1082 and 723 cm^{-1}. The $C=N^+$-H and C=N bonds may be originated from imine or imine salt due to the reaction between the amine and aldehyde or ketone (Knoepke et al. 2010; Nomura and Jones 2013). Meanwhile, the formation of P–O–C, C–N, P–O–P and P-O, which can be attributed to the degradation of phosphate esters. Simultaneously, the phosphorus-containing compound radicals including pyrophosphate radicals and phosphate ester radicals may generate from the decomposition of MFAPP, which play an important role in the interruption of free radical chain reaction. When the temperature increases, the intensity of these mentioned peaks for EP/MFAPP/PER reduce, significantly. Noteworthy, the char layer of EP/MFAPP/ORC27 exhibits a significant peak at 1709 cm^{-1} which is ascribed to C=O from the ORC27 and disappears as the temperature increases. For EP/MFAPP/ORC27, the P–O–P and P–O–C bonds still present in the char residue even at 550 °C. Strikingly, the contents of polyaromatic carbons decrease and convert to phenol and carbon in the solid phase,

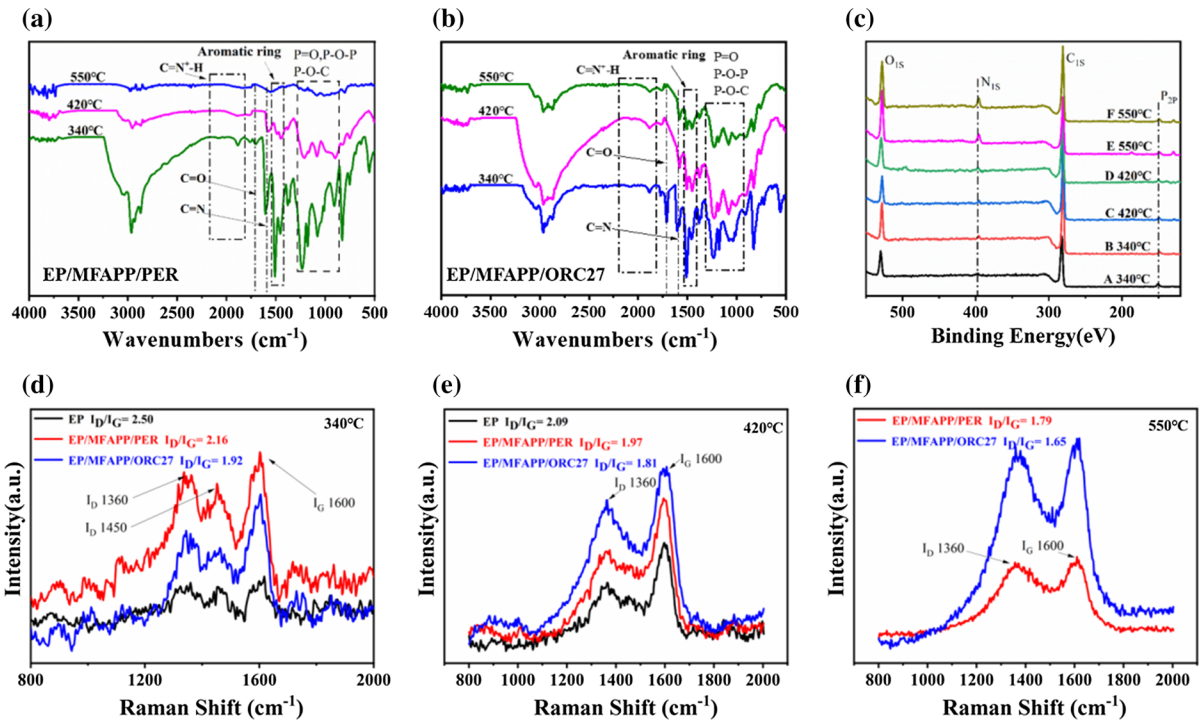

Fig. 8 Condensed phase char layer structure of epoxy thermosetting material. **a**, **b** FTIR spectra for the condensed products of different temperatures. **c** XPS spectra of the different samples: (A, C, E) EP/MFAPP/PER and (B, D, F) EP/MFAPP/ORC27. **d**, **e**, **f** Raman spectra of the exterior char residues at different temperatures

significantly. Generally, the char layers mainly consisted of graphite-like complexes and the aromatic structures bridged by P–O–P and P–O–C bonds. These cross-linked structures, such as polycyclic aromatic hydrocarbons, may further facilitate the formation of char residue by aromatization under high temperature (around 500 °C) (Shao et al. 2014b; Yan et al. 2012). The presence of these groups (e.g., C=N^+–H, C=N, P–O–C and P–O–P) in the solid char layer endow EP/MFAPP/ORC27 with significant improvement in flame retardancy compared with that of EP/MFAPP/PER.

XPS data for the condensed products in EP/MFAPP/PER and EP/MFAPP/ORC27 at different temperatures are presented at Fig. 8c to illustrate the evolution mechanism of the char formation. All samples show the presences of P, C, N and O, and their contents vary with the temperature. By the results of Table S6, the contents of N and P increase while those of C and O decrease with the increase of temperature. Detailly, XPS-peak-differentation-imitating analysis for C_{1s}, N_{1s}, O_{1s} and P_{2p} spectra of EP/MFAPP/PER and EP/MFAPP/ORC27 at 340, 420 and 550 °C are shown in Fig. S6–S8. For C_{1s} XPS spectra, the peak at 284.6 eV is assigned to the C–C and C-H bonds in aliphatic and aromatic groups, while the peak at 285.9 eV is attributed to the C-N, C–O–C and C–OH groups. Meanwhile, the peak at 287.3 eV is corresponded to C=O group of ORC27 and the peak disappears as the temperature increases to 550 °C. Compared with that of EP/MFAPP/PER, EP/MFAPP/ORC27 exhibits a higher peak intensity at 285.9 eV, indicating the presence of more carbon-containing structure in the char layer of EP/MFAPP/ORC27. As shown in N_{1s} XPS spectra for all samples, the peak at 398.6 eV is attributed to C-N or P-N group, and the peak at 400.2 and 401.4 eV is assigned to N=C and N–H bonds, respectively. Noteworthy, the peak at 400.2 eV is attributed to the formation of the imine or imine salt. For O_{1s} XPS spectra, three peaks (C=O/P=O at 531.3 eV, P-O/C-O at 532.1 eV, and C–OH and COOR at 533.2 eV) are appeared in both samples (Zhu et al. 2019). For P_{2p} XPS spectra, two characteristic peaks of the pyrophosphate or polyphosphate compounds (P-O at 133.8 eV, P=O at 134.7 eV) are appeared in two curves. Obviously, the XPS patterns of samples are good agreements with the FTIR results of EP/MFAPP/ORC27.

The contents of each binding energy of corresponding structures of carbon (C), nitrogen (N), oxygen (O), and phosphorus (P) are presented in Table S7. It is noted that the contents of C–C and C=C atoms for EP/MFAPP/ORC27 are less than those of EP/MFAPP/PER at 340 °C and 420 °C. However, EP/MFAPP/ORC27 exhibits higher content of C–C and C=C bonds at 550 °C, which indicates that a large amount of C structure remained in the char residue of EP/MFAPP/ORC27. The content of C–O–C and C–O–P atoms for EP/MFAPP/ORC27 are higher than that of EP/MFAPP/PER when the temperature increases from 340 to 420 °C, and keep a stable value at 550 °C. Generally, the C–O–C and P–O–C structures can improve the stability of the residue by bound to aromatic species (Shao et al. 2014b). When the temperature is lower than 420 °C, a dense carbon layer with C=O, C–O–C and P–O–C bonds is formed and more gas is retained (proved by FTIR and TG-MS), promoting to the expansion of the char layer. Prominently, there are abundant C=N structures in the intumescent char layer and the contents of C=N, C-N of EP/MFAPP/ORC27 are higher than EP/MFAPP/PER at 550 °C. It is well known that the thermal stability of C=N and C–N bonds is better than C=C and C–C, respectively, which results in a more stable char. Moreover, the content of P=O bond of EP/MFAPP/ORC27 is higher than that of EP/MFAPP/PER when the temperature increases from 340 to 550 °C. This result further confirms that the char layer of EP/MFAPP/ORC27 contains higher contents of phosphoric acid and poly/pyro/super-phosphoric than those of EP/MFAPP/PER. The overall effect of ORC27 in the condensed phase can promote EP to form more stable char and higher carbon residue due to its acid catalysis. Therefore, as MFAPP is incorporated, ORC27 significantly increases the char yield of EP during combustion. The char layer insulates against heat transfer and prevents oxygen from reaching the substrate, and also accumulates non-combustion gases in the condensed phase. Consequently, EP/MFAPP/ORC27 achieves higher flame retardancy performances.

Raman spectroscopy was adopted to further characterize the carbon structure of char residues. Figure 8d, e, f shows the Raman spectra of EP, EP/MFAPP/PER and EP/MFAPP/ORC27 at 340, 420 and 550 °C, respectively. The Raman spectra consist of two overlapping bands at about 1600 cm^{-1} (G band,

reflecting the graphitic structure) and 1360 cm^{-1} (D band, reflecting the amorphous structure). Basically, the R value equal to I_D/I_G provides the information to recognize the graphitization degree of char. Theoretically, samples own the higher the R value will mean that they obtain the lower graphitization degree of the char (Jian et al. 2019). The high-graphitized char can achieve improved melt strength of char layer and effectively retard the flame and protect the inner polymer matrix. During combustion, EP tends to form the amorphous structure char and displays a poor flame retardancy performance. Figure 8d, e, f also presents that R of all samples decreases with the increase of temperature and EP/MFAPP/ORC27 shows the highest graphitization degree of char. The results confirm that the introduction of IFR can improve the graphitization degree of the char, significantly. Furthermore, based on above discussion, the decomposed products of EP/MFAPP/ORC27 at 420 °C are a key factor for the high expansion char layer. Yang et al. proposed the "2D structure of fused rings" may transition to a "graphite microcrystalline structure" when the temperature is higher than 550 °C (Chen et al. 2017). Thus, R of EP/MFAPP/ORC27 and EP/MFAPP/PER decreases. It is proposed that the catalytic carbonization of ORC27 and the esterification of polyphosphoric acid can promote the formation of protective char layer and hence decrease the HRR and THR values of EP/MFAPP/ORC27. Consequently, compared with that of EP/MFAPP/PER, EP/MFAPP/ORC27 achieves 9.7-fold increase in char yield. These results demonstrate that ORC27 can effectively enhance the flame retardancy of IFR-EP, presented at Tables 1 and 2.

Prior studies have noted the compact intumescent char layer as a thermal insulation layer can restrict polymer matrix pyrolysis and inhibit the transfer of flammable gases and heat. The morphology and chemical composition of the char are of great value for the evaluation of the flame retardancy of materials (Zhao et al. 2018). SEM micrographs of the intumescent char of EP/MFAPP/PER and EP/MFAPP/ORC27 at 340, 420 and 550 °C are shown in Fig. 9. EP/MFAPP/PER exhibits a poor char layer structure with porous and multiple defect holes, which cannot prevent the release of the combustible volatile gases and oxygen permeation. However, EP/MFAPP/ORC27 obtains a homogeneous and compact char layer. These results reveal that MFAPP/ORC27 endows the EP matrix to form a protective stable and compact char layer during combustion, and thus the heat release of EP/MFAPP/ORC27 has been greatly reduced.

SEM micrographs of the intumescent char of vertical section of EP/MFAPP/PER and EP/MFAPP/ORC27 340, 420 and 550 °C are presented in Fig. 10. The intumescent carbon in the vertical section of EP/MFAPP/ORC27 is thicker than that of EP/MFAPP/PER. When the temperature increases, many holes generate in the char layer of EP/MFAPP/PER due to the excessive pyrolysis gases and amorphous structure char. Then volatile gases release from these porous char layer, resulting in an unstable char layer with a low expansion rate in the EP/MFAPP/PER. Strikingly, a smooth and compact char layer is formed in the EP/MFAPP/ORC27 and its feature has not obvious change with the increase of temperature. The stable and compact char layer can effectively isolate outside heat and oxygen, enhance the flame retardancy of EP.

Flame retardant mechanism analysis

According to the above data and discussions, herein, we propose the flame retardancy mechanism of EP/MFAPP/ORC27 which exhibits high expansion char layer, as presented at Schemes 2 and 3.

1. *The formation of heterogeneous char-forming agent (HCA).* In the initial stage (from 250 to 280 °C), part of ORC27 decomposes and forms the carbon with carboxyl content, differed with that of the PER sublimation. Interestingly, the carbon with carboxyl content may act heterogeneous effect to catalyze EP carbonization and reduces the thermal stability of EP. Consequently, with the increase of temperature (to 300 °C), more ORC27 decomposes and forms HCA sizes in the EP matrix which can improve carbonization efficiently and promote EP to form a compact char layer with aromatic crosslinked structure.
2. *The formation of IFR/EP.* As the temperature increases to about 340 °C, pyrolysis gases, such as NH_3 and phenol, generated from the decomposition of MFAPP and EP. Moreover, water vapor also emerges due to the esterification of phosphoric acid (dehydration of MFAPP) and ORC27. All these gases will expand and accelerate to establish

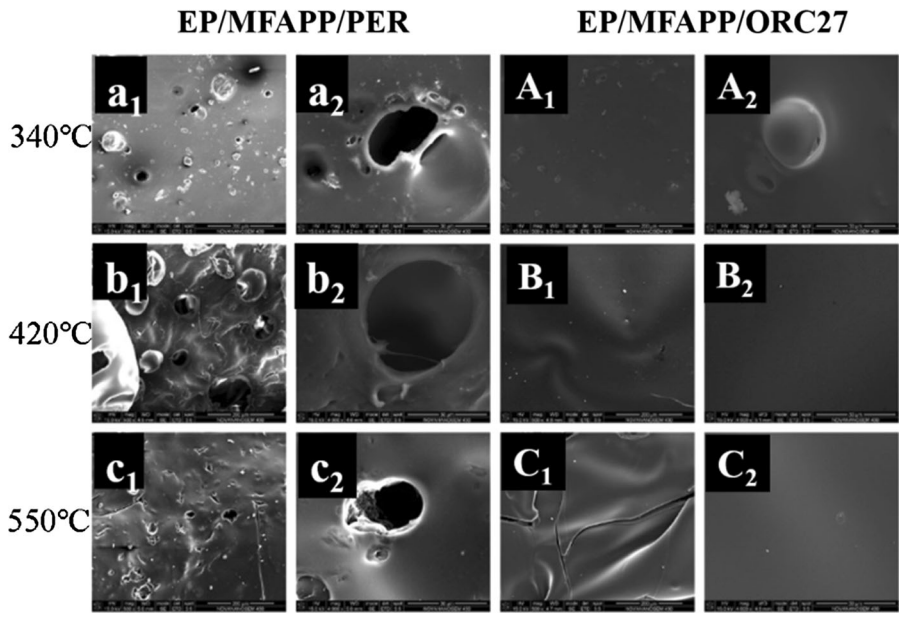

Fig. 9 SEM images of EP/MFAPP/PER ((a1, b1, c1) × 500 (a2, b2, c2) × 4000) and EP/MFAPP/ORC27((A1, B1, C1) × 500 (A2, B2, C2) × 4000) of the residues obtained from calcination test of muffle furnace

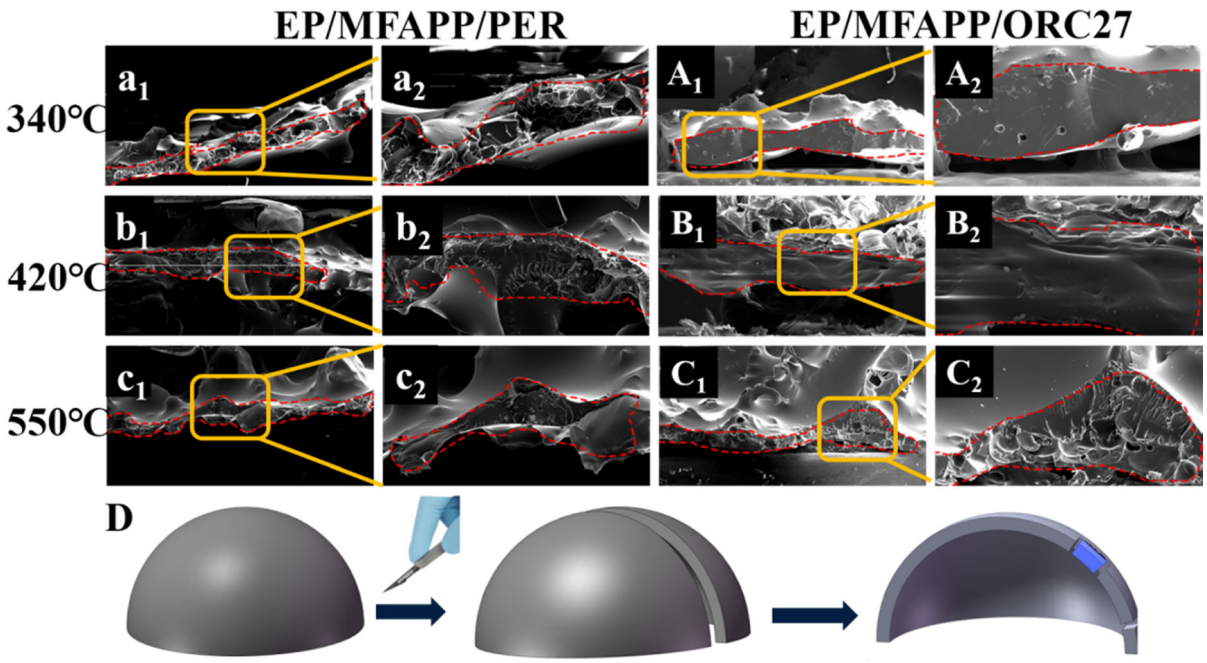

Fig. 10 SEM images of EP/MFAPP/PER ((a1, b1, c1) × 100 (a2, b2, c2) × 250) and EP/MFAPP/PORC27((A1, B1, C1) × 100 (A2, B2, C2) × 250) in the vertical section of the residues obtained from calcination test of muffle furnace. (D) A schematic of char for obtaining a vertical section of sample

an intumescent char structure of EP. Importantly, the existence of high contraction of OP^+ and O_2P^+ can accelerate the radical recombination to generate a quenching effect in the gaseous phase. Synchronously, the luxuriant P-OH bond is formed (due to esterification of phosphoric acid and ORC27) in the solid phase. Due to the HCA of ORC27, EP decomposes and forms ester structures by polycyclic aromatic stacks linked mainly with orthophosphate and pyrophosphate bridges.

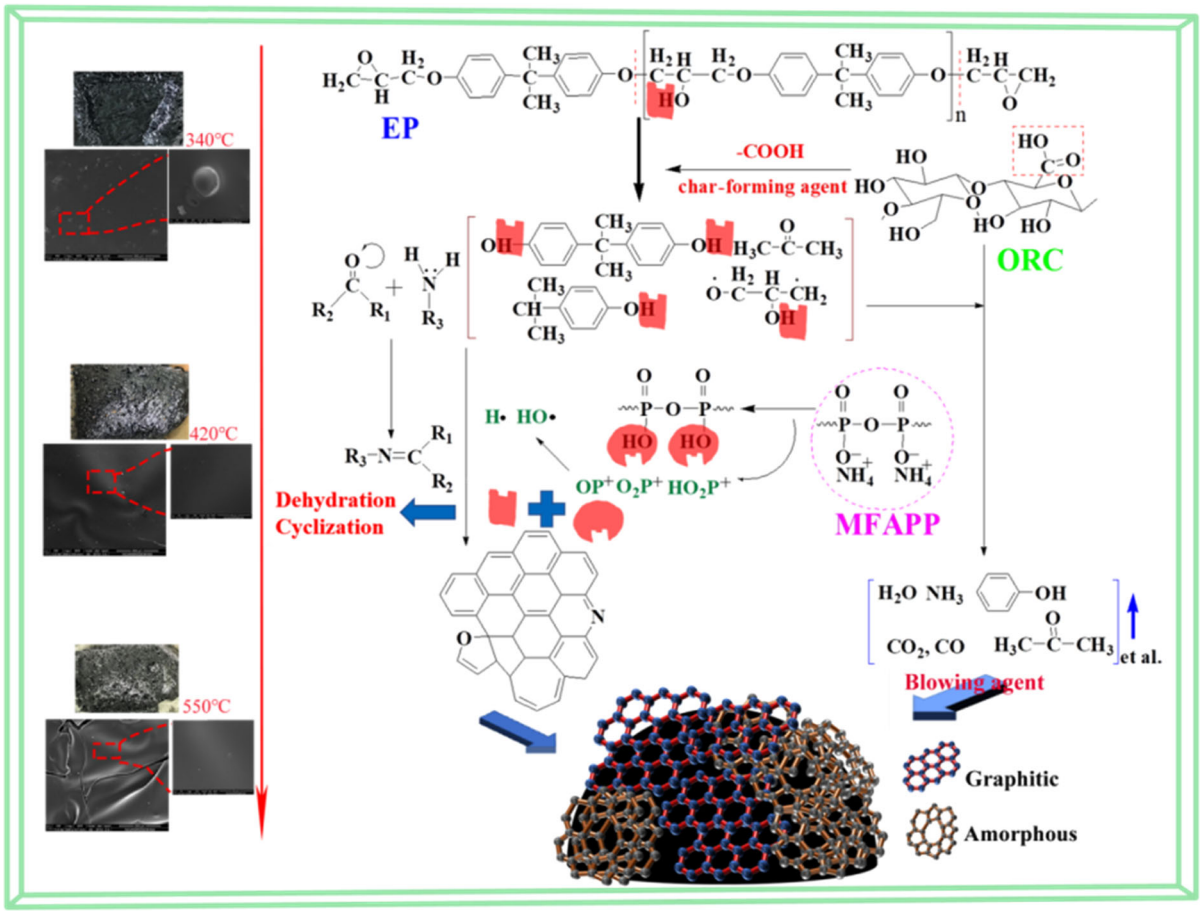

Scheme 2. Possible mechanism for charring during the combustion process of EP/MFAPP/ORC27

According to SEM, the intumescent char layer of EP/MFAPP/ORC27 is much thicker than that of EP/MFAPP/PER, which is ascribed to carboxyl groups can accelerate the transformation into carbonaceous melt of EP. Furthermore, the highly stable C=N bond originated from the polycyclic aromatic hydrocarbons (Scheme 2) presented at char layer ensures to motivate the blow molding strength (just like a balloon). Consequently, at this stage, the cross-linking reaction of carbonaceous melt occurs and matches the release amount and rate of pyrolysis gases, resulting in expanding of char from the surface of EP/MFAPP/ORC27.

3. *The formation of stable and compact char layer with high expanded ratio.* According to SEM micrographs at 420 °C of EP/MFAPP/ORC27, the char layer displays compact and expanding features, and the generation rate of pyrolysis gases decreases, significantly, compared with 340 °C corresponding data. The pyrolysis gases can act as effective blowing agents to make the melt char layer to swell without porous surfaces. Meanwhile, the P–O–C and P–C bonds in the char layer are more susceptible to cleavage due to their lower bond strength, and act as weak links during thermal degradation. The breaking of the P–O–C and P–C bonds promote the fused ring structure to convert as graphite (the I_D/I_G decreases from 1.92 to 1.81), and further generate a stable char layer with high expansion ratio. Thus, EP matrix with a protective stable and compact char layer during combustion, and the heat release of EP/MFAPP/ORC27 has been greatly reduced.
4. *The establishtion of super high expanded and compact char layers with high Flame retardant efficiency.* When the temperature increases to

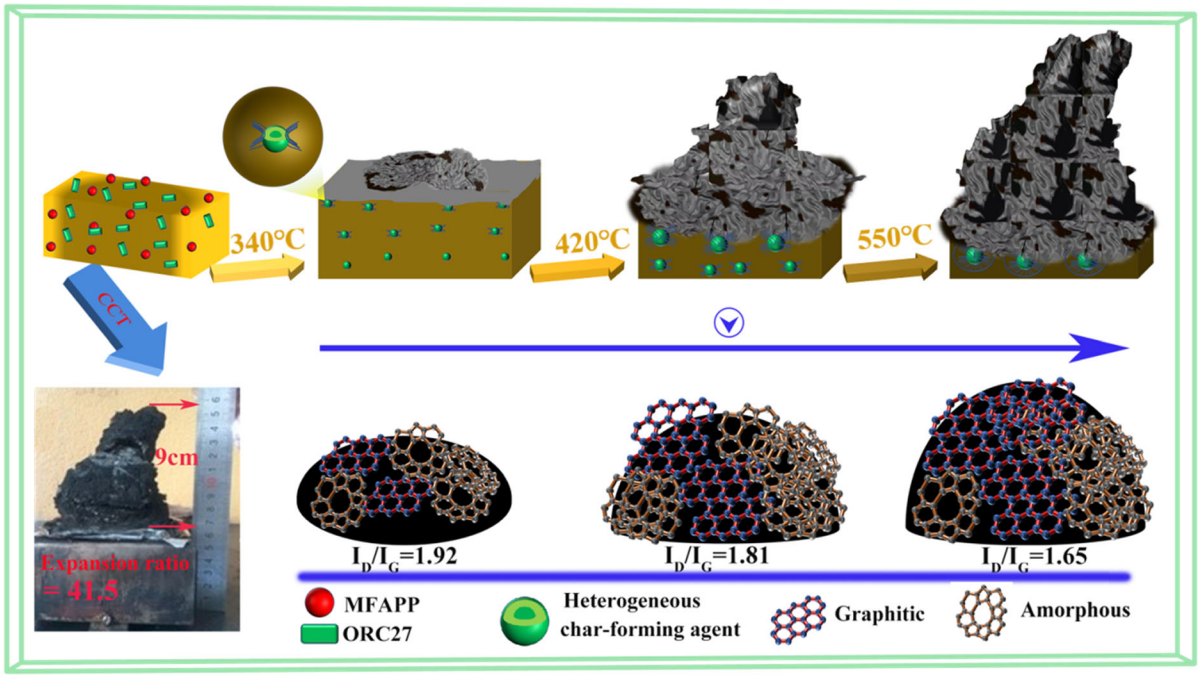

Scheme 3. The proposed flame-retardant mechanism of EP/MFAPP/ORC27

550 °C, there are not new pyrolysis gases generate for the samples and the original gases expand to high volume (Here, we support that the IFR-EP is a closed system and PV/T = K). For EP/MFAPP/ORC27, the fused ring structure may be converted to graphite (the I_D/I_G decreases to 1.65) and achieves higher char layer strength. Conversely, the intumescent char layer can hold back the expanded pyrolysis gases and form a super high expanded and compact char layer (just presented at Scheme 3). The continuous and compact structure can prevent external heat and oxygen from transmitting through the char layer and protect the unburned EP when it suffers high temperature. Furthermore, the high strength of melted char layer can maintain its stable structure under the mechanical effect of fire or convective airflow. Consequently, this new formation IFR-EP obtains high flame-retardant performances (UL-V0 with LOI of 30.3%) and super expansion ratio char layer (41.5-fold) with the significant decreases in total heat release (THR) and total smoke production (TSP), simultaneously.

Conclusion

ORC27, a novel biomass polymeric carbonization agent, mixed with MFAPP (3.75 wt%) as the intumescent flame retardants (IFR) is utilized to flame retard EP and improve its fire safety. Specifically, EP/MFAPP/ORC27 shows an increased LOI value (30.3%) and achieves a UL-94 V-0 rating. Additionally, the PHRR, THR and TSP values of EP/MFAPP/ORC27 have been decreased by 55.6%, 61.8% and 62.2%, respectively, when EP is used as the control. Surprisingly, the residual char yield significantly enhanced by 9.7-fold and obtains super expansion ratio (41.5-fold), compared with those of EP. The results prove that the introduction of ORC can remarkably improve the fire safety and flame retardancy of EP and endows EP/MFAPP/ORC27 to achieve good FRI. Based on the analysis of the gas phase and char layer structure, we propose the concept of "heterogeneous char-forming agent": ORC27 firstly decomposes and forms HCA sizes in the EP matrix which can improve carbonization efficiently and promote EP to form a compact char layer with aromatic crosslinked structure as the temperature rises. Furthermore, EP/MFAPP/ORC27 owns the optimal gas release amounts, the fused ring structure

may be converted to graphite (the I_D/I_G decreases to 1.65) and achieves higher char layer strength, which endows it to achieve good flame-retardant performances.

In summary, the significant finding to emerge from this study is proposed the new evolution law of flame retardation mechanism of IFR-EP by introduction of ORC, a novel biomass carbonization agent. This investigation develops the new applications of recycled regenerated cellulose, as well as fire safety, cheap, green and eco-friendly biomass carbonization agent to fabricate high intumescent flame-retardant performances of EP and other polymers with good FRI, super expansion and compact char layer.

Associated content

Supplementary data. Evidence for kinetic analysis; TGA evaluated the thermal stability of IFR-EP; Temperature-dependent FTIR measurements; XPS-peak-differentiation-imitating analysis. (PDF).

Acknowledgments The authors wish to acknowledge the financial support of the National Natural Science Foundation of China (No. 51773068), SKL of Bio-Fibers and Eco-Textiles (Qingdao University) K2019-05, and the Fund Research Grant for Science and Technology in Guangzhou (202002030143), China.

Compliance with ethical standards

Conflict of interest The authors declare no competing financial interest.

References

Alongi J, Di Blasio A, Milnes J, Malucelli G, Bourbigot S, Kandola B, Camino G (2015) Thermal degradation of DNA, an all-in-one natural intumescent flame retardant. Polym Degrad Stab 113:110–118. https://doi.org/10.1016/j.polymdegradstab.2014.11.001

Alongi J, Ferruti P, Manfredi A, Carosio F, Feng ZX, Hakkarainen M, Ranucci E (2019) Superior flame retardancy of cotton by synergetic effect of cellulose-derived nano-graphene oxide carbon dots and disulphide-containing polyamidoamines. Polym Degrad Stab. https://doi.org/10.1016/j.polymdegradstab.2019.108993

Bourbigot S, Duquesne S (2007) Fire retardant polymers: recent developments and opportunities. J Mater Chem 17:2283–2300. https://doi.org/10.1039/b702511d

Bourbigot S, Le Bras M, Duquesne S, Rochery M (2004) Recent advances for intumescent polymers. Macromol Mater Eng 289:499–511. https://doi.org/10.1002/mame.200400007

Camino G, Costa L, Trossarelli L (1984) Study of the mechanism of intumescence in fire retardant polymers: part II—mechanism of action in polypropylene-ammonium polyphosphate-pentaerythritol mixtures. Polym Degrad Stab 7:25–31

Camino G, Costa L, Trossarelli L (1985) Study of the mechanism of intumescence in fire retardant polymers: part VI—mechanism of ester formation in ammonium polyphosphate-pentaerythritol mixtures. Polym Degrad Stab 12:213–228. https://doi.org/10.1016/0141-3910(85)90090-4

Chen YQ, Zhang X, Chen W, Yang HP, Chen HP (2017) The structure evolution of biochar from biomass pyrolysis and its correlation with gas pollutant adsorption performance. Bioresour Technol 246:101–109. https://doi.org/10.1016/j.biortech.2017.08.138

Costes L, Laoutid F, Brohez S, Dubois P (2017) Bio-based flame retardants: when nature meets fire protection. Mater Sci Eng R 117:1–25. https://doi.org/10.1016/j.mser.2017.04.001

Ding HY, Huang K, Li SH, Xu LN, Xia JL, Li M (2017) Synthesis of a novel phosphorus and nitrogen-containing bio-based polyol and its application in flame retardant polyurethane foam. J Anal Appl Pyrol 128:102–113. https://doi.org/10.1016/j.jaap.2017.10.020

Feng YZ, He CG, Wen YF, Ye YS, Zhou XP, Xie XL, Mai YW (2018) Superior flame retardancy and smoke suppression of epoxy-based composites with phosphorus/nitrogen co-doped graphene. J Hazard Mater 346:140–151. https://doi.org/10.1016/j.jhazmat.2017.12.019

Flynn JH, Wall LA (1966) A quick, direct method for the determination of activation energy from thermogravimetric data. J Polym Ence Part C Polym Lett 4(5):323–328. https://doi.org/10.1002/pol.1966.110040504

Gu H et al (2016) An overview of multifunctional epoxy nanocomposites. J Mater Chem C 4:5890–5906

Ji XY, Chen DY, Wang QW, Shen JB, Guo SY (2018) Synergistic effect of flame retardants and carbon nanotubes on flame retarding and electromagnetic shielding properties of thermoplastic polyurethane. Compos Sci Technol 163:49–55. https://doi.org/10.1016/j.compscitech.2018.05.007

Jian RK, Ai YF, Xia L, Zhao LJ, Zhao HB (2019) Single component phosphamide-based intumescent flame retardant with potential reactivity towards low flammability and smoke epoxy resins. J Hazard Mater 371:529–539. https://doi.org/10.1016/j.jhazmat.2019.03.045

Jin FL, Li X, Park SJ (2015) Synthesis and application of epoxy resins: a review. J Ind Eng Chem 29:1–11. https://doi.org/10.1016/j.jiec.2015.03.026

Jung D, Bhattacharyya D (2018) Keratinous fiber based intumescent flame retardant with controllable functional compound loading. ACS Sustain Chem Eng 6:13177–13184. https://doi.org/10.1021/acssuschemeng.8b02756

Kalali EN, Wang X, Wang DY (2015) Functionalized layered double hydroxide-based epoxy nanocomposites with improved flame retardancy and mechanical properties.

J Mater Chem A 3:6819–6826. https://doi.org/10.1039/C5TA00010F

Ke CH et al (2010) Synergistic effect between a novel hyperbranched charring agent and ammonium polyphosphate on the flame retardant and anti-dripping properties of polylactide. Polym Degrad Stab 95:763–770. https://doi.org/10.1016/j.polymdegradstab.2010.02.011

Knoepke LR, Nemati N, Koeckritz A, Brueckner A, Bentrup U (2010) Reaction monitoring of heterogeneously catalyzed hydrogenation of imines by coupled ATR-FTIR, UV/Vis, and Raman spectroscopy. Chemcatchem 2:273–280. https://doi.org/10.1002/cctc.200900273

Laoutid F, Bonnaud L, Alexandre M, Lopez-Cuesta JM, Dubois P (2009) New prospects in flame retardant polymer materials: from fundamentals to nanocomposites. Mater Sci Eng R 63:100–125. https://doi.org/10.1016/j.mser.2008.09.002

Li XL, Zhang FH, Jian RK, Ai YF, Ma JL, Hui GJ, Wang DY (2019) Influence of eco-friendly calcium gluconate on the intumescent flame-retardant epoxy resin: flame retardancy, smoke suppression and mechanical properties. Compos B Eng 176:107200. https://doi.org/10.1016/j.compositesb.2019.107200

Liu Y, Zhao J, Deng CL, Chen L, Wang DY, Wang YZ (2011) Flame-retardant effect of sepiolite on an intumescent flame-retardant polypropylene system. Ind Eng Chem Res 50:2047–2054. https://doi.org/10.1021/ie101737n

Liu Y, Yu Q, Fang Z, Zhang Y (2015) The effect of a novel intumescent flame retardant-functionalized montmorillonite on the thermal stability and flammability of EVA. Polym Polym Compos 23:345–350. https://doi.org/10.1177/096739111502300507

Manfredi A, Carosio F, Ferruti P, Ranucci E, Alongi J (2018) Linear polyamidoamines as novel biocompatible phosphorus-free surface-confined intumescent flame retardants for cotton fabrics. Polym Degrad Stab 151:52–64. https://doi.org/10.1016/j.polymdegradstab.2018.02.020

Nie SB, Song L, Guo YQ, Wu K, Xing WY, Lu HD, Hu Y (2009) Intumescent flame retardation of starch containing polypropylene semibiocomposites: flame retardancy and thermal degradation. Ind Eng Chem Res 48:10751–10758. https://doi.org/10.1021/ie9012198

Nomura A, Jones CW (2013) Amine-functionalized porous silicas as adsorbents for aldehyde abatement. ACS Appl Mater Inter 5:5569–5577. https://doi.org/10.1021/am400810s

Ozawa T (1965) A new method of analyzing thermogravimetric data. Bull Chem Soc Jpn 38(11):1881–1886. https://doi.org/10.1246/bcsj.38.1881

Pappalardo S, Russo P, Acierno D, Rabe S, Schartel B (2016) The synergistic effect of organically modified sepiolite in intumescent flame retardant polypropylene. Eur Polym J 76:196–207. https://doi.org/10.1016/j.eurpolymj.2016.01.041

Peng HQ, Zhang SD, Yin Y, Jiang SH, Mo WJ (2017) Fabrication of c-6 position carboxyl regenerated cotton cellulose by H2O2 and its promotion in flame retardency of epoxy resin. Polym Degrad Stab 142:150–159. https://doi.org/10.1016/j.polymdegradstab.2017.05.026

Qi DP, Liu Y, Liu ZY, Zhang L, Chen XD (2017) Design of architectures and materials in in-plane micro-supercapacitors: current status and future challenges. Adv Mater. https://doi.org/10.1002/adma.201602802

Shao ZB, Deng C, Tan Y, Yu L, Chen MJ, Chen L, Wang YZ (2014b) Ammonium polyphosphate chemically-modified with ethanolamine as an efficient intumescent flame retardant for polypropylene. J Mater Chem A 2:13955–13965. https://doi.org/10.1039/c4ta02778g

Shao ZB, Deng C, Tan Y, Chen MJ, Chen L, Wang YZ (2014a) An efficient mono-component polymeric intumescent flame retardant for polypropylene: preparation and application. ACS Appl Mater Int 6:7363–7370. https://doi.org/10.1021/am500789q

Shen ZQ, Chen L, Lin L, Deng CL, Zhao J, Wang YZ (2013) Synergistic effect of layered nanofillers in intumescent flame-retardant epdm: montmorillonite versus layered double hydroxides. Ind Eng Chem Res 52:8454–8463. https://doi.org/10.1021/ie4010546

Song P, Xu L, Guo Z, Zhang Y, Fang Z (2008) Flame-retardant-wrapped carbon nanotubes for simultaneously improving the flame retardancy and mechanical properties of polypropylene. J Mater Chem 18:5083–5091. https://doi.org/10.1039/b808309f

Su XQ, Yi YW, Tao J, Qi HQ (2012) Synergistic effect of zinc hydroxystannate with intumescent flame-retardants on fire retardancy and thermal behavior of polypropylene. Polym Degrad Stab 97:2128–2135. https://doi.org/10.1016/j.polymdegradstab.2012.08.017

Tan Y, Shao ZB, Chen XF, Long JW, Chen L, Wang YZ (2015) Novel multifunctional organic inorganic hybrid curing agent with high flame-retardant efficiency for epoxy resin. ACS Appl Mater Inter 7:17919–17928. https://doi.org/10.1021/acsami.5b04570

Tan Y, Shao ZB, Yu LX, Long JW, Qi M, Chen L, Wang YZ (2016a) Piperazine-modified ammonium polyphosphate as monocomponent flame-retardant hardener for epoxy resin: flame retardance, curing behavior and mechanical property. Polym Chem UK 7:3003–3012. https://doi.org/10.1039/c6py00434b

Tan Y, Shao ZB, Yu LX, Xu YJ, Rao WH, Chen L, Wang YZ (2016b) Polyethyleneimine modified ammonium polyphosphate toward polyamine-hardener for epoxy resin: thermal stability, flame retardance and smoke suppression. Polym Degrad Stab 131:62–70. https://doi.org/10.1016/j.polymdegradstab.2016.07.004

Vahabi H, Kandola BK, Saeb MR (2019) Flame retardancy index for thermoplastic composites. Polymers 11(3):407. https://doi.org/10.3390/polym11030407

Vandersall HL (1971) Intumescent coating systems, their development and chemistry. J Fire Flammabl 2(1971):97–140

Wang X, Hu YA, Song L, Xuan SY, Xing WY, Bai ZM, Lu HD (2011) Flame retardancy and thermal degradation of intumescent flame retardant poly(lactic acid)/starch biocomposites. Ind Eng Chem Res 50:713–720. https://doi.org/10.1021/ie1017157

Wang X, Song L, Yang HY, Xing WY, Kandola B, Hua Y (2012) Simultaneous reduction and surface functionalization of graphene oxide with POSS for reducing fire hazards in epoxy composites. J Mater Chem 22:22037–22043. https://doi.org/10.1039/c2jm35479a

Wang X, Kalali EN, Wan JT, Wang DY (2017a) Carbon-family materials for flame retardant polymeric materials. Prog Polym Sci 69:22–46. https://doi.org/10.1016/j.progpolymsci.2017.02.001

Wang ZJ, Liu YF, Li J (2017b) Regulating effects of nitrogenous bases on the char structure and flame retardancy of polypropylene/intumescent flame retardant composites. ACS Sustain Chem Eng 5:2375–2383. https://doi.org/10.1021/acssuschemeng.6b02712

Wang TS, Li LP, Wang QW, Xie GJ, Guo CG (2019) Castor oil based UV-cured coatings using thiol-ene click reaction for thermal degradation with flame retardance. Ind Crop Prod. https://doi.org/10.1016/j.indcrop.2019.111798

Wen JH, Yin Y, Peng XF, Zhang SD (2019) Using H_2O_2 to selectively oxidize recyclable cellulose yarn with high carboxyl content. Cellulose 26:2699–2713. https://doi.org/10.1007/s10570-018-2217-1

Xing WY, Zhang P, Song L, Wang X, Hu Y (2014) Effects of alpha-zirconium phosphate on thermal degradation and flame retardancy of transparent intumescent fire protective coating. Mater Res Bull 49:1–6. https://doi.org/10.1016/j.materresbull.2013.08.033

Xu ZZ, Huang JQ, Chen MJ, Tan Y, Wang YZ (2013) Flame retardant mechanism of an efficient flame-retardant polymeric synergist with ammonium polyphosphate for polypropylene. Polym Degrad Stab 98:2011–2020. https://doi.org/10.1016/j.polymdegradstab.2013.07.010

Xu L, Liu X, An ZH, Yang R (2019) EG-based coatings for flame retardance of shape stabilized phase change materials. Polym Degrad Stab 161:114–120. https://doi.org/10.1016/j.polymdegradstab.2019.01.020

Yan YW, Chen L, Jian RK, Kong S, Wang YZ (2012) Intumescence: an effect way to flame retardance and smoke suppression for polystryene. Polym Degrad Stab 97:1423–1431. https://doi.org/10.1016/j.polymdegradstab.2012.05.013

Yang L, Cheng WL, Zhou J, Li HL, Wang XL, Chen XD, Zhang ZY (2014) Effects of microencapsulated APP-II on the microstructure and flame retardancy of PP/APP-II/PER composites. Polym Degrad Stab 105:150–159. https://doi.org/10.1016/j.polymdegradstab.2014.04.014

Yang YX, Haurie L, Wen JH, Zhang SD, Ollivier A, Wang DY (2019) Effect of oxidized wood flour as functional filler on the mechanical, thermal and flame-retardant properties of polylactide biocomposites. Ind Crop Prod 130:301–309. https://doi.org/10.1016/j.indcrop.2018.12.090

Yang W et al (2020) Nanoparticles of polydopamine for improving mechanical and flame-retardant properties of an epoxy resin. Compos B Eng. https://doi.org/10.1016/j.compositesb.2020.107828

Zhang SD, Zhang YR, Wang XL, Wang YZ (2009) High carbonyl content oxidized starch prepared by hydrogen peroxide and its thermoplastic application. Starch Starke 61:646–655. https://doi.org/10.1002/star.200900130

Zhang LX, Liu ZH, Cui GL, Chen LQ (2015a) Biomass-derived materials for electrochemical energy storages. Prog Polym Sci 43:136–164. https://doi.org/10.1016/j.progpolymsci.2014.09.003

Zhang SD, Liu F, Peng HQ, Peng XF, Jiang SH, Wang JS (2015b) Preparation of novel c-6 position carboxyl corn starch by a green method and its application in flame retardance of epoxy resin. Ind Eng Chem Res 54:11944–11952. https://doi.org/10.1021/acs.iecr.5b03266

Zhang W, Fina A, Cuttica F, Camino G, Yang RJP (2016) Blowing-out effect in flame retarding epoxy resins: insight by temperature measurements during forced combustion. Polym Degrad Stab 131:82–90. https://doi.org/10.1016/j.polymdegradstab.2016.07.002

Zhang W, Fina A, Ferraro G, Yang R (2018) FTIR and GCMS analysis of epoxy resin decomposition products feeding the flame during UL 94 standard flammability test. Application to the understanding of the blowing-out effect in epoxy/polyhedral silsesquioxane formulations. J Anal Appl Pyrol 135:271–280. https://doi.org/10.1016/j.jaap.2018.08.026

Zhang L et al (2019) Nickel metal-organic framework derived hierarchically mesoporous nickel phosphate toward smoke suppression and mechanical enhancement of intumescent flame retardant wood fiber/poly(lactic acid) composites. ACS Sustain Chem Eng 7:9272–9280. https://doi.org/10.1021/acssuschemeng.9b00174

Zhao X, Guerrero FR, Llorca J, Wang DYJ (2016) New superefficiently flame-retardant bioplastic poly (lactic acid): flammability, thermal decomposition behavior, and tensile properties. ACS Sustain Chem Eng 4:202–209. https://doi.org/10.1021/acssuschemeng.5b00980

Zhao D, Wang J, Wang XL, Wang YZ (2018) Highly thermostable and durably flame-retardant unsaturated polyester modified by a novel polymeric flame retardant containing Schiff base and spirocyclic structures. Chem Eng J 344:419–430. https://doi.org/10.1016/j.cej.2018.03.102

Zhou X et al (2019) Design of hierarchical NiCo-LDH@PZS hollow dodecahedron architecture and application in high-performance epoxy resin with excellent fire safety. ACS Appl Mater Int 11:41736–41749. https://doi.org/10.1021/acsami.9b16482

Zhu ZM, Wang LX, Dong LP (2019) Influence of a novel P/N-containing oligomer on flame retardancy and thermal degradation of intumescent flame-retardant epoxy resin. Polym Degrad Stab 162:129–137. https://doi.org/10.1016/j.polymdegradstab.2019.02.021